

Article

AgTx2-GFP, Fluorescent Blocker Targeting Pharmacologically Important $K_v1.x$ ($x = 1, 3, 6$) Channels

Alexandra L. Primak^{1,2}, Nikita A. Orlov^{1,2}, Steve Peigneur³, Jan Tytgat³, Anastasia A. Ignatova¹, Kristina R. Denisova^{1,2}, Sergey A. Yakimov¹, Mikhail P. Kirpichnikov^{1,2}, Oksana V. Nekrasova¹, and Alexey V. Feofanov^{1,2,*}

¹ Shemyakin-Ovchinnikov Institute of Bioorganic Chemistry, Russian Academy of Sciences, 117997 Moscow, Russia

² Faculty of Biology, Lomonosov Moscow State University, 119234 Moscow, Russia

³ Toxicology and Pharmacology, Campus Gasthuisberg O&N2, University of Leuven (KU Leuven), Herestraat 49, P.O. Box 922, B-3000 Leuven, Belgium

* Correspondence: avfeofanov@yandex.ru

Abstract: The growing interest in potassium channels as pharmacological targets has stimulated the development of their fluorescent ligands (including genetically encoded peptide toxins fused with fluorescent proteins) for analytical and imaging applications. We report on the properties of agitoxin 2 C-terminally fused with enhanced GFP (AgTx2-GFP) as one of the most active genetically encoded fluorescent ligands of potassium voltage-gated $K_v1.x$ ($x = 1, 3, 6$) channels. AgTx2-GFP possesses subnanomolar affinities for hybrid KcsA- $K_v1.x$ ($x = 3, 6$) channels and a low nanomolar affinity to KcsA- $K_v1.1$ with moderate dependence on pH in the 7.0–8.0 range. Electrophysiological studies on oocytes showed a pore-blocking activity of AgTx2-GFP at low nanomolar concentrations for $K_v1.x$ ($x = 1, 3, 6$) channels and at micromolar concentrations for $K_v1.2$. AgTx2-GFP bound to $K_v1.3$ at the membranes of mammalian cells with a dissociation constant of 3.4 ± 0.8 nM, providing fluorescent imaging of the channel membranous distribution, and this binding depended weakly on the channel state (open or closed). AgTx2-GFP can be used in combination with hybrid KcsA- $K_v1.x$ ($x = 1, 3, 6$) channels on the membranes of *E. coli* spheroplasts or with $K_v1.3$ channels on the membranes of mammalian cells for the search and study of nonlabeled peptide pore blockers, including measurement of their affinity.

Keywords: agitoxin 2; GFP; voltage-gated K_v1 channels; KcsA- K_v1 channels; affinity; confocal; patch clamp; oocytes; Neuro 2a cells

Key Contribution: Agitoxin 2 C-terminally tagged with GFP is shown to be a high-affinity fluorescent blocker of voltage-gated $K_v1.x$ ($x = 1, 3, 6$) channels. As demonstrated, it can be used to search for peptide pore blockers and to study them in combination with hybrid KcsA- $K_v1.x$ ($x = 1, 3, 6$) channels expressed in bacteria or with $K_v1.3$ channel expressed in mammalian cells, as well as for the fluorescent imaging of $K_v1.3$ channels in mammalian cells.



Citation: Primak, A.L.; Orlov, N.A.; Peigneur, S.; Tytgat, J.; Ignatova, A.A.; Denisova, K.R.; Yakimov, S.A.; Kirpichnikov, M.P.; Nekrasova, O.V.; Feofanov, A.V. AgTx2-GFP, Fluorescent Blocker Targeting Pharmacologically Important $K_v1.x$ ($x = 1, 3, 6$) Channels. *Toxins* **2023**, *15*, 229. <https://doi.org/10.3390/toxins15030229>

Received: 14 February 2023

Revised: 14 March 2023

Accepted: 16 March 2023

Published: 18 March 2023



Copyright: © 2023 by the authors. Licensee MDPI, Basel, Switzerland. This article is an open access article distributed under the terms and conditions of the Creative Commons Attribution (CC BY) license (<https://creativecommons.org/licenses/by/4.0/>).

1. Introduction

Many peptide toxins from scorpion venoms are potent and specific blockers of potassium channels [1,2], which are tetrameric transmembrane proteins with a central ion-conducting pore [3]. The toxins bind at the outer vestibule of a channel, occluding the pore with a lysine residue. The main targets of scorpion peptide toxins are voltage-gated $K_v1.x$ channels, calcium-activated K^+ channels (K_{Ca}), and $K_v11.x$ channels [1,2,4]. The affinity profile of each peptide toxin usually comprises a limited set of K^+ -channel isoforms, suggesting that scorpion toxins are able to discriminate a few targets from dozens of different K^+ channels [1,5]. For example, the OSK1 toxin from the scorpion *Orthochirus scrobiculosus*

is a high-affinity blocker of $K_v1.1$ and $K_v1.3$ channels [6], is moderately active on $K_v1.2$ [6], is weakly active on $K_v1.6$ and $K_{Ca3.1}$ channels [6,7] and is not active on $K_v1.4$, $K_v1.5$, $K_v1.7$, $K_v3.1$, $K_v3.2$, K_v11 , $K_{Ca1.1}$, $K_{Ca2.1}$, $K_{Ca2.2}$, and $K_{Ca2.3}$ channels [6–8]. The BeKm1 toxin from the scorpion *Mesobuthus eupeus* is a potent blocker of the $K_v11.1$, $K_v11.2$, $K_v11.3$, and $K_v12.1$ channels [9] and is not active on the $K_v2.3$, $K_v7.1$, $K_v7.2$, $K_v7.4$, K_v10 , $K_{Ca1.1}$, $K_{Ca2.1}$, $K_{Ca2.2}$, and $K_{Ca3.1}$ channels [6–8]. Some scorpion toxins are highly selective, showing high-affinity binding to a single target channel, such as, for example, the $K_v1.3$ channel blockers agitoxin 1 and Vm24 [10,11] or the $K_v1.2$ channel blocker MeKTx11-1 [12].

The properties of scorpion toxins have made them a unique tool for studying K^+ channels, which are abundant in almost all types of cells and tissues [6,13,14]. The structure and functions of K^+ channels have been clarified with such peptides as margatoxin, charybdotoxin, agitoxin 2 (AgTx2), iberiotoxin, scyllatoxin, Vm24, HsTX1[R14A], and some others [1,13–18]. Charybdotoxin, a potent blocker of several K_v1 and K_{Ca} channels, has been used to study structural determinants of toxin–channel interactions [19,20]. AgTx2 and margatoxin helped to prove the involvement of $K_v1.1$ and $K_v1.3$ channels in the mechanisms of retinal ganglion cell degeneration [21] and to identify the expression of $K_v1.3$ in activated microglial cells as a probable reason for the modulation of microglia proliferation [22]. When applying the $K_v1.3$ channel peptide blocker HsTX1[R14A] to microglial cells, it was found that the levels of TNF-alpha, IL-6, and nitric oxide production associated with microglia-mediated neuroinflammation depended on the $K_v1.3$ channel activity [18]. The Vm24 toxin assisted in a study of T_{EM} cell response to $K_v1.3$ blocking [17]. By using iberiotoxin, it was demonstrated that blocking the $K_{Ca1.1}$ channel enhanced cell migration, thus indicating the role of the $K_{Ca1.1}$ channel in intestinal epithelial restitution [15]. The compounds and mechanisms modulating the expressions of small-conductance Ca^{2+} -activated K^+ channels in human neuroblastoma cells were studied using scyllatoxin [16].

The growing interest in potassium channels as pharmacological targets associated with autoimmune, cancer, and neurological diseases [23–29] has provoked a major effort in using peptide toxins as a pharmacophore for engineering advanced peptides with increased selectivity and affinity to target channels [30–33]. It was shown that therapy-oriented selective peptide blockers can be developed using phage display based on a library of scorpion toxin sequences [34]. Moreover, this interest has stimulated the development and refinement of a wide variety of labeled blockers for different analytical and imaging applications. Radio- or fluorescently labeled peptide blocker derivatives are successfully used in radioligand or fluorescence-based binding assays, as well as in studies on K^+ channel traffic and distribution [35].

In many cases, the labeling strategy includes the construction of a mutated peptide (by inserting Tyr or Cys residue) with retained biological activity, followed by the iodination of Tyr with ^{125}I [36,37], and the labeling of Cys with [3H]-N-ethylmaleimide [38] or with thiol-reactive fluorescent dyes [39,40]. Other approaches are based on the labeling of the N-terminal amino group with an organic fluorophore during solid-phase synthesis of the peptide [41–43] or the “blind” labeling of one of several Lys residues, which are present in the peptide, with an amino-reactive organic fluorophore [44]. In the latter case, the separation of labeled derivatives and the selection of the most active ones followed by the determination of the modified Lys residue are required.

An alternative strategy to create fluorescently labeled peptide blockers is the production of genetically encoded peptide toxins fused with fluorescent proteins (FPs) [7,45–47]. Currently, FPs used for such constructions are limited to TagRFP (hereinafter RFP) [48] and enhanced GFP [49], while a list of peptide blockers includes MgTx, OSK1, hongotoxin 1, and AgTx2. Studies of these FP-tagged toxins (FP-Txs) reveal high (nanomolar and even subnanomolar) affinities of FP-Txs to particular isoforms of K_v1 channels. It has been proved that FP-Tx binding to channels is accompanied by channel blocking. The relative affinities of FP-Txs to target channels may vary compared to those of a native toxin. Indeed, the affinities of FP-Txs to K_v1 channels are lower than those of free toxins, but the extent of affinity reduction varies in a complicated way for particular combinations

of FPs and toxins [7,45–47], for different FPs fused with the same toxin [7,46], and for different modes of tagging (N- or C-terminal) [46,47]. For example, N-terminal tagging of AgTx2 with RFP retained, in general, the relative affinities to the $K_v1.1$, $K_v1.3$, and $K_v1.6$ channels but reduced moderately the relative affinity toward the $K_v1.2$ channel [7]. In contrast, N-terminal tagging of AgTx2 with GFP resulted in considerable enhancement of the selectivity to the $K_v1.3$ binding site compared to the $K_v1.1$ and $K_v1.6$ binding sites [46]. This ligand, GFP-AgTx2, is the first known example of an engineered ligand in which high selectivity for the target K_v1 channel was achieved by simply fusing a peptide toxin with a bulky FP. It is noteworthy that the permutation of GFP from the N- to the C-terminus of AgTx2 restored interaction with the $K_v1.1$ and $K_v1.6$ binding sites [46].

These data clearly indicate that, when developing new FP-Txs based on various FPs and toxins, the spectrum of activities of new molecular constructions should be carefully studied to assess the effect of bulky FPs on the binding properties of the Tx moieties. FPs of different origins (for example, jellyfish or coral) have a specific surface charge and topology of charged residues that can affect the interactions of FP-Txs with channels.

Recently, we reported the design and preliminary properties of AgTx2 C-terminally fused with GFP (AgTx2-GFP) [46]. Using hybrid KcsA- $K_v1.x$ ($x = 1, 3, 6$) channels expressed in the inner membranes of *E. coli* cells, it was demonstrated that AgTx2-GFP interacted specifically with the pore blocker binding sites of $K_v1.x$ ($x = 1, 3, 6$) channels and was displaced from these complexes by known peptide blockers of these channels.

The present work is devoted to a detailed study of the properties of AgTx2-GFP. Affinities of AgTx2-GFP to hybrid KcsA- $K_v1.x$ ($x = 1, 3, 6$) channels on the membranes of *E. coli* spheroplasts, to mammalian $K_v1.x$ ($x = 1–3, 6$) channels on the membranes of *Xenopus laevis* oocytes, and to the human $K_v1.3$ channel on the membranes of mammalian cells are evaluated. It is demonstrated that combinations of AgTx2-GFP and *E. coli* spheroplasts expressing KcsA- $K_v1.x$ ($x = 1, 3, 6$) channels or AgTx2-GFP and mammalian cells expressing the $K_v1.3$ channel can be used for the search and study of peptide pore blockers. It is demonstrated that AgTx2-GFP is a high-affinity fluorescent probe for the imaging of $K_v1.3$ channels in cells.

2. Results and Discussion

2.1. Interactions of AgTx2-GFP with KcsA- $K_v1.x$ ($x = 1, 3, 6$) Channels

AgTx2-GFP was obtained by fusing GFP with the C-terminus of AgTx2 by means of a flexible 20 amino acid linker (GSGGSGSGGTGGAGGATST) [46].

To characterize quantitatively the previously revealed interactions of AgTx2-GFP with the pore blocker binding sites of $K_v1.x$ ($x = 1, 3, 6$) channels, the concentration dependences of AgTx2-GFP binding to the hybrid potassium channels KcsA- $K_v1.x$ ($x = 1, 3, 6$) expressed in the inner membranes of *E. coli* cells were measured (Figure 1). KcsA- $K_v1.x$ ($x = 1, 3, 6$) channels comprised the pore blocker outer-binding sites of corresponding eukaryotic channels, which were transferred to the bacterial KcsA channel (Figure 1c) [44,50,51]. As shown earlier, the affinities of peptide pore blockers to KcsA- $K_v1.x$ ($x = 1, 3, 6$) channels were similar to their affinities to corresponding eukaryotic K_v1 channels [52].

The confocal microscopy analysis of AgTx2-GFP interactions with KcsA- $K_v1.x$ ($x = 1, 3, 6$) channels on the membranes of spheroplasts prepared from *E. coli* cells revealed saturable binding that occurred in subnanomolar (KcsA- $K_v1.3$) and low nanomolar (KcsA- $K_v1.1$ and KcsA- $K_v1.6$) concentration ranges (Figure 1d–f). This AgTx2-GFP binding was reversible, and peptide blockers of $K_v1.x$ ($x = 1, 3, 6$) channels displaced AgTx2-GFP from spheroplasts bearing KcsA- $K_v1.x$ ($x = 1, 3, 6$) channels [46]. In addition, AgTx2-GFP binding to the *E. coli* membrane itself, as well as to the KcsA channel embedded in the *E. coli* membrane, was negligible compared to its binding to spheroplasts bearing KcsA- $K_v1.x$ ($x = 1, 3, 6$) channels [46]. These findings allowed us to validly fit experimental data using Equation (1) (Figure 1d–f) and to determine the dissociation constants K_d of AgTx2-GFP complexes with KcsA- $K_v1.x$ ($x = 1, 3, 6$) channels (Table 1).

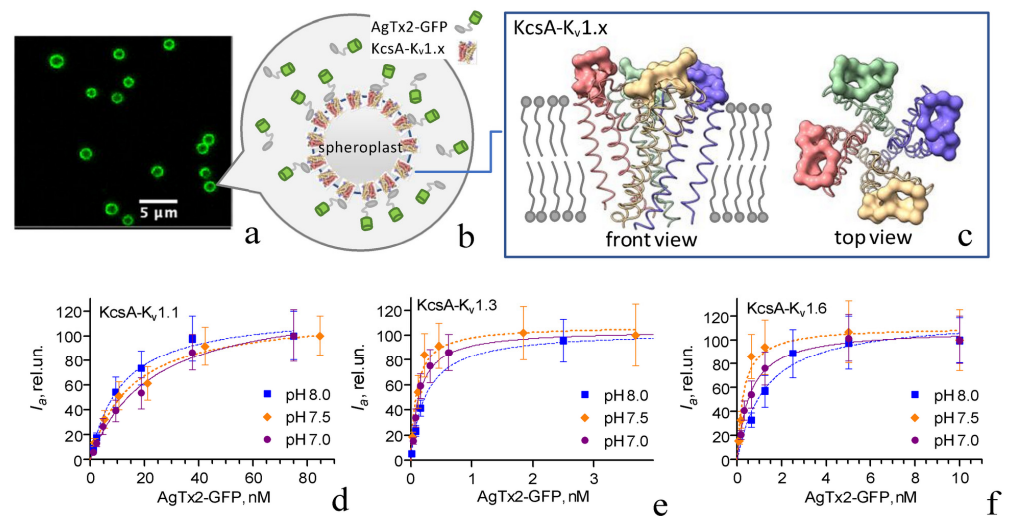


Figure 1. Interactions of AgTx2-GFP with hybrid KcsA-K_v1.x (x = 1, 3, 6) channels on the membranes of *E. coli* spheroplasts. (a) Typical confocal image of AgTx2-GFP bound to KcsA-K_v1.x on the membranes of *E. coli* spheroplasts. (b) A scheme of AgTx2-GFP interaction with a spheroplast expressing KcsA-K_v1.x channels on the plasma membrane. (c) A scheme of the structure of a hybrid KcsA-K_v1.x channel (based on PDB:1F6G of the KcsA channel). Subunits of the KcsA-K_v1.x channel are shown in different colors. KcsA residues are shown in ribbon presentation. Positions of K_v1.x residues transferred to KcsA are shown in cloud presentation. (d–f) Concentration dependences of AgTx2-GFP binding to hybrid KcsA-K_v1.x (x = 1, 3, 6) channels at pH 7.0, 7.5, and 8.0. I_a values are presented as means \pm SD.

Table 1. Dissociation constants K_d (nM) of AgTx2-GFP complexes with KcsA-K_v1.x (x = 1, 3, 6) channels at different pH values.

pH	KcsA-K _v 1.1	KcsA-K _v 1.3	KcsA-K _v 1.6
7.0	23 \pm 4	0.14 \pm 0.02	0.60 \pm 0.06
7.5	15 \pm 3 *	0.10 \pm 0.01 *	0.30 \pm 0.08 *
8.0	12 \pm 2 *	0.25 \pm 0.02 *	1.3 \pm 0.4 *

* $p < 0.05$, comparison with K_d at pH 7.0.

The affinity of AgTx2-GFP to the hybrid channels reduced in the manner of KcsA-K_v1.3 > KcsA-K_v1.6 >> KcsA-K_v1.1 and was found to be moderately sensitive to pH in the neutral to slightly basic pH range (Table 1). The affinity of AgTx2-GFP to KcsA-K_v1.1 was the lowest at pH 7.0 and increased at higher pH values (Table 1). The affinities of AgTx2-GFP to KcsA-K_v1.3 and KcsA-K_v1.6 were highest at pH 7.5 and decreased at both pH 7.0 and pH 8.0 (Table 1). Since the pK_a values of most amino acids are far from the pH range of 7–8 and cysteines of AgTx2 are in the form of cystines, the histidine residues with $pK_a = 6.3$ were the most likely candidates whose protonation–deprotonation equilibrium affected the K_d of the studied complexes. H34 of AgTx2 and H58 of the binding site of KcsA-K_v1.1 could be responsible for the revealed pH dependence, while the absence of histidine residues in the binding sites of KcsA-K_v1.3 and KcsA-K_v1.6 could be a reason for the variation in the character of pH dependences of these hybrid channels compared to KcsA-K_v1.1 (Table 1). Additionally, a decrease in the protonation state of the N-terminal amino group of AgTx2, which occurred at the increase in pH from 7.0 to 8.0, could affect peptide binding.

As compared to previously studied FP-Txs, AgTx2-GFP was inferior to RFP-AgTx2 and GFP-OSK1 in its affinity to KcsA-K_v1.1 (Figure 2a) [7]. At the same time, AgTx2-GFP surpassed all the studied FP-Txs in its reported affinities to KcsA-K_v1.3 (Figure 2a) and KcsA-K_v1.6 [7]. It should be noted that K_d were measured for AgTx2-GFP at an ionic strength that was noticeably higher than in the measurements of K_d values for other FP-Txs.

A decrease in the ionic strength of the solution can increase the affinities of peptide blockers to the binding sites of K_v1 channels due to the considerable role of electrostatic interactions in the formation of a peptide–channel complex [50,51].

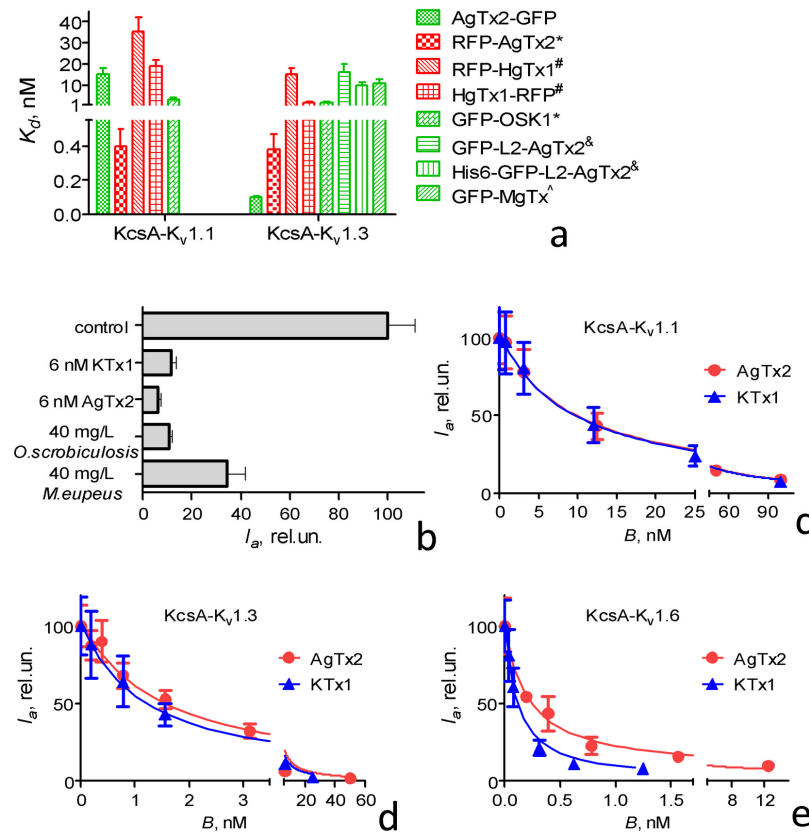


Figure 2. AgTx2-GFP as a ligand of KcsA-K_v1.x ($x = 1, 3, 6$) channels. (a) Comparison of dissociation constants (K_d , mean \pm SEM) of KcsA-K_v1.x ($x = 1, 3$) complexes with AgTx2-GFP and with previously studied FP-tagged pore blockers. * [7], # [47], & [46], ^ [45]. (b) Displacement of AgTx2-GFP (5 nM) from complexes with KcsA-K_v1.3 (control) by kaliotoxin 1 (KTx1), AgTx2, and the components of crude venoms of *Mesobuthus eupeus* and *Orthochirus scrobiculosus* scorpions. (c–e) Displacement of AgTx2-GFP from complexes with KcsA-K_v1.1 (c), KcsA-K_v1.3 (d), and KcsA-K_v1.6 (e) by different concentrations B of KTx1 and AgTx2. I_a —relative fluorescence intensity of AgTx2-GFP bound to spheroplasts bearing KcsA-K_v1.x ($x = 1, 3, 6$) channels. Concentrations of AgTx2-GFP in the experiments with KcsA-K_v1.1, KcsA-K_v1.3, and KcsA-K_v1.6 were 80, 8, and 2 nM, respectively. I_a values are presented as means \pm SD.

AgTx2-GFP could be displaced from complexes with KcsA-K_v1.x ($x = 1, 3, 6$) not only by pure, specific peptide pore blockers [46], but also by complex mixtures of natural peptides, such as crude scorpion venoms containing pore blockers (Figure 2b). This result confirms that AgTx2-GFP in combination with KcsA-K_v1.x ($x = 1, 3, 6$) channels could be used to search for K_v1 channel pore blockers among individual compounds and in complex natural extracts and venoms. As demonstrated earlier [51], the targeted detection of specific activity using a combination of a fluorescent ligand and KcsA-K_v1.x ($x = 1, 3, 6$) channels facilitated significantly the targeted isolation of individual peptide blockers of K_v1 channels from venoms.

Displacement of AgTx2-GFP from the complexes with KcsA-K_v1.x ($x = 1, 3, 6$) channels by the nonlabeled peptide blocker occurred due to the competitive binding to the K_v1 channel binding site. A quantitative analysis of such displacement by the studied peptide blocker for the particular channels (Figure 2c–e) allowed the estimation of the peptide concentration, which displaced 50% of AgTx2-GFP from the complexes (DC_{50}),

and the calculation of the apparent dissociation constant K_{ap} of the studied peptide blocker (Equations (2) and (3)) [44]. The K_{ap} values determined for KTx1 and AgTx2 using the AgTx2-GFP/KcsA-K_v1.x ($x = 1, 3, 6$) bioengineering analytical systems (Table 2) allowed us to conclude that AgTx2-GFP was applicable as a component of these systems for the study of peptide blockers and their affinities to K_v1 channels.

Table 2. Apparent dissociation constants K_{ap} (nM) of AgTx2 and KTx1 complexes with KcsA-K_v1.x ($x = 1, 3, 6$) channels.

Toxin	KcsA-K _v 1.1	KcsA-K _v 1.3	KcsA-K _v 1.6
AgTx2	3.7 ± 0.8	0.039 ± 0.007	0.027 ± 0.004
KTx1	3.8 ± 0.8	0.032 ± 0.006	0.016 ± 0.002

The affinities of AgTx2 to KcsA-K_v1.3 and KcsA-K_v1.6 estimated with AgTx2-GFP (Table 2) are in general agreement with the data on AgTx2 activity (IC_{50} , blocker concentration inhibiting current through the channel by 50%) reported in electrophysiological studies: 4 pM [10], 50 pM [34], 200 pM [53], and 170 pM (Figure 3, Table 3) for K_v1.3 and 37 pM [10] and 600 pM (Figure 3, Table 3) for K_v1.6. The measured affinity of AgTx2 to KcsA-K_v1.1 (Table 2) is close to the previously reported K_{ap} value determined with another fluorescent ligand [51], as well as to recent IC_{50} values of 2 nM [7] and 4.2 nM (Figure 3, Table 3) obtained in electrophysiological studies of the K_v1.1 channel. At the same time, earlier electrophysiological studies have reported much lower IC_{50} values (44 pM [10] and 130 pM [34]) for inhibition of the K_v1.1 channel by AgTx2, and the reason for these differences is unclear.

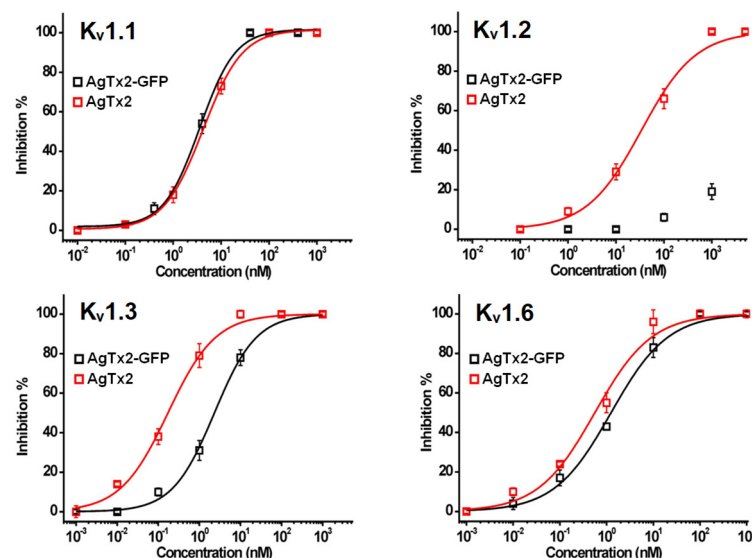


Figure 3. Concentration dependences of current inhibition through K_v1.x ($x = 1–6$) channels in oocytes by AgTx2 and AgTx2-GFP measured with a two-electrode voltage clamp technique. Currents through K_v1.x ($x = 1–6$) channels were induced by 250 ms depolarization to 0 mV followed by a 250 ms pulse to -50 mV from a holding potential of -90 mV. Data are presented as means \pm SEM and fitted with Equation (4) (see Materials and Methods).

The K_{ap} values of KTx1 complexes with KcsA-K_v1.1 and KcsA-K_v1.3 (Table 2) correlated to the IC_{50} values reported for KTx1 complexes with K_v1.1 (1.1 nM) and K_v1.3 (0.1 nM) [34]. To our best knowledge, there are no quantitative electrophysiological data on the inhibition of K_v1.6 by KTx1, but only qualitative ones [54].

Table 3. Concentrations of AgTx2 and AgTx2-GFP that induced 50% inhibition of the current through $K_v1.x$ ($x = 1-3,6$) channels in oocytes (IC_{50} , nM).

Ligand	$K_v1.1$	$K_v1.2$	$K_v1.3$	$K_v1.6$
AgTx2-GFP	3.5 ± 0.5 ¹	- ²	2.31 ± 0.22	1.30 ± 0.15
AgTx2	4.2 ± 0.3	34 ± 6	0.17 ± 0.03	0.60 ± 0.11

¹ mean \pm SEM. ² IC_{50} was not achieved. 1 μ M AgTx2-GFP provided 19% inhibition.

2.2. Electrophysiological Studies of AgTx2-GFP

According to the data on electrophysiological measurements on oocytes, AgTx2-GFP was a pore blocker of $K_v1.x$ ($x = 1-3, 6$) channels (Figure 3). Its affinity to the channels decreased in the following manner: $K_v1.6 > K_v1.3 > K_v1.1 \gg K_v1.2$ (Table 3). C-terminal attachment of GFP did not affect the affinity of AgTx2 to $K_v1.1$ but decreased its activity by two, ten, and more than thirty times to $K_v1.6$, $K_v1.3$, and $K_v1.2$, respectively, thus changing noticeably the natural pharmacological profile of AgTx2 (Table 3). A significant decrease in the affinity of AgTx2-GFP to the $K_v1.2$ channel could be associated with the disturbance of strong interactions between the channel and amino acid residues near the C-terminus of the peptide by a volumetric fluorescent protein. According to 1H-NMR studies, these could be the Lys32 and His34 of AgTx2 forming a salt bridge with Asp355 and hydrophobic contacts with the Gly378, Asp379, and Val381 of the channel, respectively [55].

Finally, $K_v1.6$, $K_v1.3$, and $K_v1.1$ differed in affinity to AgTx2-GFP by less than three times, which made AgTx2-GFP a high-affinity fluorescent marker of K_v1 channels of a wide spectrum of action.

The affinities of AgTx2-GFP to hybrid KcsA- $K_v1.x$ ($x = 1, 3, 6$) channels (Table 1) and corresponding $K_v1.x$ ($x = 1, 3, 6$) channels (Table 3) differed noticeably, reflecting the influences of buffer composition and the structural differences of hybrid and natural channels on the binding of the bulky AgTx2-GFP ligand. Apparently, the FP (in our case, GFP) could participate in interactions with amino acid residues of the channel surrounding or beyond the natural binding site of the peptide blocker and, thus, modulate the overall affinity of the ligand to the channel. Differences in the amino acid compositions of KcsA- $K_v1.x$ and the corresponding $K_v1.x$ channels beyond the binding site led to differences in interactions with GFP moiety and, finally, to differences in the stability of the complexes.

2.3. Interaction of AgTx2-GFP with $K_v1.3$ on Mammalian Cell Membranes

Recently, we created a plasmid encoding a natural (M1-D52)-truncated variant of the $K_v1.3$ channel [56] fused with red fluorescent protein mKate2 (mKate2- $K_v1.3$), which is effectively expressed in the plasma membranes of mammalian cells and retains voltage-gated K^+ conductivity and the ability to bind peptide pore blockers [42]. Our studies show that AgTx2-GFP bound to the membrane of Neuro 2A and HEK293 cells expressing the mKate2- $K_v1.3$ channel (Figures 4 and S1). The $K_v1.3$ channel was obviously a target of AgTx2-GFP in these cells since no binding of AgTx2-GFP to cells was observed in the absence of mKate2- $K_v1.3$ channels (Figure S2). Moreover, AgTx2 displaced AgTx2-GFP from the surfaces of cells expressing the mKate2- $K_v1.3$ channel, indicating competition of these ligands for the pore blocker binding site of $K_v1.3$ (Figures 4 and S1).

To characterize the affinity of AgTx2-GFP to $K_v1.3$ on the membranes of mammalian cells, we measured the concentration dependence of AgTx2-GFP binding to mKate2- $K_v1.3$ -expressing Neuro 2A cells using confocal microscopy and calculated the ratios (R_{av}) of the fluorescent intensity of bound AgTx2-GFP to the fluorescent intensity of membranous mKate2- $K_v1.3$ at different concentrations of added AgTx2-GFP (Figure 5a). Previously, it was shown that the analysis of such a dependence using Equation (5) allowed one to calculate the K_d of the formed complexes [42]. The measurements were carried out after a 30 min incubation of the cells with AgTx2-GFP when the complexation process reached equilibrium (Figure S3). The calculated K_d of AgTx2-GFP complexes with $K_v1.3$ on the

Neuro 2A cell membranes was 3.4 ± 0.8 nM, which was consistent with the data of the electrophysiological measurements (Table 3).

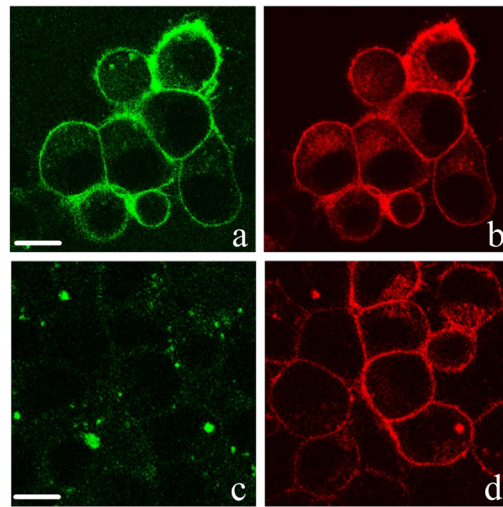


Figure 4. Confocal imaging of the interaction of AgTx2-GFP (green) with Neuro 2A cells expressing mKate2-K_v1.3 (red). (a,b) Distribution of AgTx2-GFP (8 nM, 30 min incubation) bound to K_v1.3 on the membranes of cells. Bar is 10 μm. (c,d) Concurrent inhibition of the binding of AgTx2-GFP (8 nM) to K_v1.3 by AgTx2 (8 nM). Incubation time of cells with the ligands was 30 min. Bar is 10 μm.

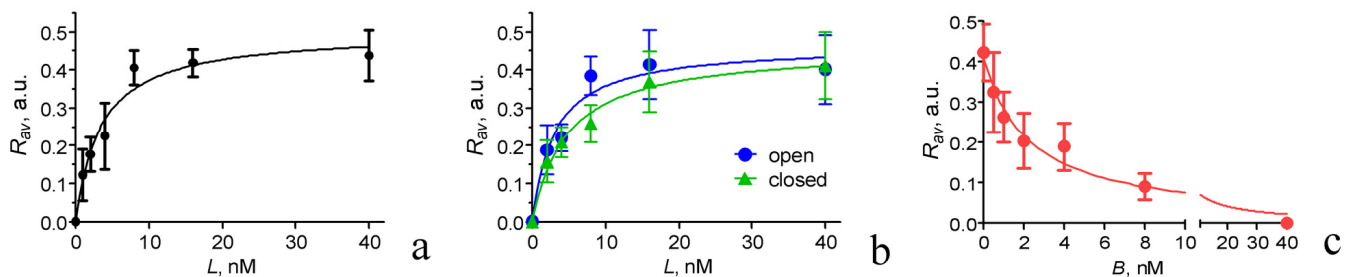


Figure 5. Quantitative analysis of AgTx2-GFP interaction with the K_v1.3 channel on the membranes of Neuro 2A cells expressing mKate2-K_v1.3 channels. (a) Concentration dependence of AgTx2-GFP binding to K_v1.3 measured in a culture medium as the dependence of R_{av} (mean \pm SD) on the concentration L of added AgTx2-GFP (see Section 4 for details). (b) Comparison of AgTx2-GFP binding to K_v1.3 (R_{av} , mean \pm SEM) on the membranes of Neuro 2A cells expressing mKate2-K_v1.3 channels in conditions that favored either open or closed states of the channels. Measurements were performed in a buffer (20 mM HEPES pH 7.4, 0.9 mM CaCl₂, 0.5 mM MgCl₂, and 0.1% bovine serum albumin) containing either 150 mM KCl or 150 mM NaCl and 4 mM KCl, thus either favoring open or maintaining closed states of the channels, respectively. (c) Concentration dependence of the displacement of AgTx2-GFP (8 nM) from complexes with K_v1.3 channels by AgTx2 measured as the dependence of R_{av} (mean \pm SD) on the concentration B of added AgTx2 (see Section 4 for details).

It is worth mentioning that the measurements of the affinities of AgTx2-GFP to the K_v1.3 channel with the fluorescent cell-based assay (Figure 5a) and electrophysiological approach (Figure 3) were performed at different states of the channel—closed and open, respectively. Similar values of K_d and IC_{50} obtained in these measurements allowed us to assume that the affinity of AgTx2-GFP to K_v1.3 depended weakly, if at all, on the state of the channel (open or closed). To verify this assumption using the same technique, we compared changes in AgTx2-GFP binding to K_v1.3 on the cell membranes in buffers containing either 150 mM NaCl or 150 mM KCl (Figure 5b). The presence of NaCl in the outer medium maintained the predominantly closed state of the channels, while KCl induced depolarization of the plasma membrane and the opening of the channels. The

calculated K_d values of the AgTx2-GFP complexes with open and closed $K_v1.3$ channels were 3 ± 1 and 4.7 ± 0.8 nM, respectively. The difference between these K_d values was insignificant, thus confirming the assumption made.

Considering a probable application of AgTx2-GFP as a fluorescent ligand for the study of interactions of various peptide blockers with $K_v1.3$ channels on mammalian cells, we measured the concentration dependence of the competitive binding of AgTx2 to $K_v1.3$ at a constant concentration (8 nM) of AgTx2-GFP added to cells following an earlier developed procedure [42]. An analysis of the displacement of AgTx2-GFP from complexes with mKate2- $K_v1.3$ by increasing concentrations of AgTx2 allowed one to calculate the AgTx2 concentration displacing 50% of the AgTx2-GFP from the complexes (DC_{50} , Equation (6)) and the K_{ap} of the complexes between AgTx2 and $K_v1.3$ (Equation (7)). The calculated K_{ap} was 0.7 ± 0.2 nM, which is in a good agreement with the electrophysiological data presented in Table 3 and published earlier [10,34,53].

The data obtained allowed one to conclude that AgTx2-GFP was suitable for the fluorescent imaging of $K_v1.3$ channels in mammalian cells, as well as for recognizing $K_v1.3$ blockers among the studied peptide toxins and assessing their affinity for $K_v1.3$, when AgTx2-GFP was used in combination with mammalian cells expressing fluorescent (FP-tagged) $K_v1.3$ channels. Such studies are also useful at an earlier stage of the selection of a candidate drug among peptides. In vitro cell experiments are a mandatory part of preclinical studies for any candidate drug. The initial selection and study of peptide blockers is often performed in buffer solutions by means of electrophysiological techniques on *Xenopus* oocytes or radioligand analyses on isolated membranes. These results need to be verified in a more complex and natural environment, where background proteolytic activity and various nonspecific interactions with the components of a mammalian cell growth medium can affect the blocker–channel interactions.

AgTx2-GFP is a high-affinity fluorescent ligand of the $K_v1.1$, $K_v1.3$, and $K_v1.6$ channels whose increased expression and activity are associated with a number of diseases. The $K_v1.3$ channel is involved in the development of autoimmune or neuroimmune inflammation through the induction of pro-inflammatory response and the activation of T lymphocytes or microglial cells, respectively [57,58]. CD4+ effector memory T cells mediate many autoimmune diseases, including multiple sclerosis, type-I diabetes mellitus, and rheumatoid arthritis. The selective blockage of $K_v1.3$ channels in these cells inhibits their proliferation and cytokine production, thereby contributing to a reduction in inflammation and providing a therapeutic effect [23]. The pathogenesis of oncological diseases, such as breast and prostate cancers, pancreatic ductal adenocarcinoma, or B-type chronic lymphocytic leukemia, are associated with the upregulation of $K_v1.3$ channel expression [59]. The inhibition of $K_v1.3$ channels by either small organic blockers or peptide toxins from animal venoms results in a significant therapeutic effect without major side effects [60]. Inherited loss-of-function mutations of the $K_v1.1$ channel in humans are associated with episodic ataxia type I [61], while some other deletions or mutations of the $K_v1.1$ and $K_v1.2$ channels provoke epilepsy [62]. Although the blockage of $K_v1.1$ and $K_v1.2$ channels has no therapeutic value in cases of increased excitability of neurons, the inhibition of $K_v1.1$ channels in inhibitory (demyelinated) axons is known to improve neuronal conduction in multiple sclerosis [63]. While the physiological role of the $K_v1.6$ channel, which is widely expressed in the central nervous system and peripheral neurons, is still poorly determined, the localization of $K_v1.6$ in microglial cells in the striatum suggests its potential role in neuroinflammation and striatal disorders, such as Parkinson's disease [64].

Comparing the prospects of the best organic fluorophores and FPs for the fluorescent labeling of peptide ligands of K_v1 channels, it can be stated that organic fluorophores are usually brighter and more photostable, but the differences are gradually being leveled due to the extensive development of new FP variants [65–67]. For many laboratories that are familiar with the technology of recombinant proteins, FP-Tx production is simpler than the synthesis of fluorophore-labeled peptide blockers, especially because the recombinant production of FP-Txs usually provides a high yield of a fully active ligands with properly

formed disulfide bonds without additional refolding of the product [46]. It should be noted that even small organic fluorophores can unpredictably modulate the affinities and pharmacological profiles of peptide blockers of K_v1 channels [43], not only FPs [46].

3. Conclusions

AgTx2-GFP was shown to have subnanomolar affinities to hybrid KcsA- $K_v1.3$ and KcsA- $K_v1.6$ channels and a nanomolar affinity to the KcsA- $K_v1.1$ channel (Table 1). Since these affinities were slightly sensitive to pH in the 7.0–8.0 range, a constant pH value should be maintained in studies to increase the reproducibility of the results. AgTx2-GFP could be used as a component of the analytical system based on hybrid KcsA- $K_v1.x$ ($x = 1, 3, 6$) channels expressed in the membranes of *E. coli* cells [52] for the study of peptide blockers and the evaluation of their affinities to K_v1 channels (Table 2). Data from electrophysiological measurements on oocytes indicated that AgTx2-GFP was a pore blocker of $K_v1.x$ ($x = 1, 3, 6$) channels possessing nanomolar activity (Table 3). AgTx2-GFP could be equally used as a high-affinity fluorescent marker of the $K_v1.6$, $K_v1.3$, and $K_v1.1$ channels. Nanomolar activity of AgTx2-GFP was preserved for both open and closed $K_v1.3$ channels expressed in the membranes of mammalian cells (Figure 5). Fluorescent imaging of $K_v1.3$ channels and studies of the activities of $K_v1.3$ peptide blockers are potential applications of AgTx2-GFP in mammalian cells.

Data on the properties of AgTx2-GFP and previously studied FP-Txs [7,45–47] have shown that FP-Txs can be considered as a reliable alternative to peptide blockers labeled with organic fluorophores for the fluorescent imaging of K_v1 channels, as well as for a number of analytical applications. FPs can modulate the pharmacological profiles of peptide blockers of K_v1 channels, maintaining a high (nanomolar) affinity to some of the target channels or even enhancing considerably the ligand selectivity for a particular channel. A wide variety of peptide blockers differing in the repertoire of amino acid residues interacting with K_v1 channels, together with a wide variety of FPs having not only different colors but also distinct compositions and distributions of surface-charged residues, can provide multiple combinations of FP-Txs with valuable properties. The design and study of such FP-Txs is still at an early stage.

4. Materials and Methods

4.1. Reagents

AgTx2-GFP was produced as described previously [46]. Its concentration in an aqueous solution was determined using the molar extinction coefficient of $55,000 \text{ M}^{-1} \text{ cm}^{-1}$ at 489 nm. Recombinant peptides of KTx1 and AgTx2 were obtained as described earlier [68]. Concentrations of KTx1 and AgTx2 were measured in an aqueous solution containing 20% acetonitrile and 0.1% trifluoroacetic acid using molar extinction coefficients (at 214 nm) of $49,300$ and $49,200 \text{ M}^{-1} \text{ cm}^{-1}$, respectively.

The plasmid pmKate2-KCNA3-del was obtained as described earlier [42].

Crude venoms of *M. eupeus* and *O. scrobiculosus* scorpions were a kind gift from Dr. Alexander Vassilevski.

4.2. Experiments with KcsA and KcsA- $K_v1.x$ ($x = 1, 3, 6$) Channels

Hybrid KcsA- $K_v1.x$ ($x = 1, 3, 6$) channels were expressed in *E. coli* cells as described earlier [44,50,51]. Cells were transformed to spheroplasts following the protocol described earlier [44]. For AgTx2-GFP binding experiments, spheroplasts expressing KcsA- $K_v1.x$ ($x = 1, 3, 6$) channels were incubated (500–1000 cells/ μL , 37°C , 2 h) with AgTx2-GFP (0.02–85 nM) in a buffer containing 50 mM NaCl, 50 mM Tris-HCl (pH 7.0, 7.5, or 8.0), 0.1% BSA, 0.25 M sucrose, 10 mM MgCl_2 , 4 mM KCl, and 0.3 mM EDTA. Displacement of AgTx2-GFP from complexes with KcsA- $K_v1.x$ ($x = 1, 3, 6$) channels was analyzed by incubating spheroplasts with a constant concentration of AgTx2-GFP and increasing concentrations of AgTx2 or KTx1 peptides (0.04–100 nM) at 37°C for 2 h. In similar experiments with scorpion venoms, AgTx2-GFP was added to spheroplasts, together with crude venom

(40 mg/L) of *M. eupeus* or *O. scrobiculosus* scorpions. Concentrations of AgTx2-GFP in the experiments with KcsA-K_v1.1, KcsA-K_v1.3, and KcsA-K_v1.6 were 80, 8, and 2 nM, respectively. Measurements were performed at pH 7.5 in the buffer described above.

Spheroplasts were imaged with a laser scanning confocal microscope LSM710 (Zeiss, Germany) equipped with an α Plan-Apochromat 100 \times /1.46 oil immersion objective (excitation at 488 nm, detection in the 495–590 nm range, 0.2 μ m lateral and 2 μ m axial resolutions). Fluorescent images of spheroplasts were analyzed as reported earlier [44,50,51]. Fluorescence intensity of AgTx2-GFP bound to KcsA-K_v1.x (x = 1, 3, 6) was estimated for each analyzed spheroplast and averaged over 150–250 spheroplasts to obtain the I_a value (\pm SD).

K_d values of AgTx2-GFP complexes with KcsA-K_v1.x (x = 1, 3, 6) were calculated from the measured I_a dependencies on the concentration L of added AgTx2-GFP using the following equation:

$$I_a = I_s L / (K_d + L) \quad (1)$$

where I_s is the I_a value at the saturation of binding.

Data on the displacement of AgTx2-GFP from complexes with KcsA-K_v1.x (x = 1, 3, 6) by a nonlabeled peptide blocker were fitted with the following equation:

$$I_a = I_0 / (1 + B / DC_{50}) \quad (2)$$

where B is the concentration of the added nonlabeled peptide, DC_{50} is the concentration of the nonlabeled peptide displacing 50% of AgTx2-GFP from the complex with the KcsA-K_v1.x channel, and I_0 is the I_a at $B = 0$.

The K_{ap} value of the nonlabeled peptide blocker was calculated using the Cheng–Prusoff equation:

$$K_{ap} = DC_{50} / (1 + L / K_d) \quad (3)$$

where L is the constant concentration of AgTx2-GFP.

The K_d and K_{ap} values were averaged over three independent experiments and presented as means \pm SEM.

4.3. Electrophysiological Experiments

Stage V–VI oocytes were harvested from an anesthetized female *X. laevis* frog following the KU Leuven guidelines for animal welfare, as described earlier [69,70]. The oocytes were incubated in ND96 solution (96 mM NaCl, 2 mM KCl, 1.8 mM CaCl₂, 2 mM MgCl₂, 5 mM HEPES, pH 7.4) containing 50 mg/L gentamycin sulfate.

Expressions of rat K_v1.1, K_v1.2, and K_v1.6 and human K_v1.3 channels in *X. laevis* oocytes were performed as described previously [71]. Transcription of linearized plasmids bearing K_v1 genes was performed using either T7 or SP6 mMMESSAGE mMACHINE transcription kits (Invitrogen, CA, USA).

Two-electrode voltage clamp recording was performed at 18–22 °C using a Geneclamp 500 amplifier (Molecular Devices, CA, USA) and an Axon pClamp data acquisition system (Molecular Devices, CA, USA), as described earlier [72]. Whole-cell currents from oocytes were recorded 1–4 days after injection of 50 nl of cRNA (1 g/L). Current and voltage electrodes were filled with 3 M KCl, and their resistances were kept between 0.7 and 1.5 M Ω . The bath solution was ND96. The induced currents were filtered at 0.5 kHz and sampled at 2 kHz using a four-pole low-pass Bessel filter. Leak was subtracted using a–P/4 protocol. Currents through K_v1.x (x = 1–3, 6) channels were induced by 250 ms depolarization to 0 mV followed by a 250 ms pulse to –50 mV from a holding potential of –90 mV.

Concentration dependences of the inhibition of currents through K_v1.x (x = 1–3, 6) channels by AgTx2-GFP and AgTx2 were measured and fitted with the Hill equation:

$$y = 100 / (1 + (IC_{50} / C)^h) \quad (4)$$

where y is the relative decrease (%) in current amplitude at the concentration C of a pore blocker, IC_{50} is the pore blocker concentration inducing a 50% decrease in the current amplitude, and h is the Hill coefficient. The Hill coefficients for all the measured dependences were found to be close to 1 (not shown). Concentrations of AgTx2-GFP and AgTx2 varied from 1 nM to 1 μ M. Experimental data obtained in several independent experiments are presented as means \pm SEM ($n \geq 3$).

4.4. Experiments with Neuro2a Cells Expressing $K_v1.3$ Channels

Mouse Neuro-2A cells (from the collection of the Institute of Cytology RAS, Russia) were grown (37 °C, 5% CO₂) in Dulbecco's modified Eagle's medium DMEM/F12 (Paneco, Russia) supplemented with 5% fetal bovine serum (FBS, HyClone, UT, USA) and 2 mM L-glutamine (complete medium). Cells were replanted every 72 h. Cells used in the experiments were from the 5–20 passages. Transient transfection with the pmKate2-KCNA3-del plasmid was performed using GenJector-U reagent (Molecta, Russia) at nearly 50% confluence according to the manufacturer's protocol. All the experiments with cells were performed within 24 h after transfection. Cells were incubated with AgTx2-GFP (1–40 nM) in complete medium at 37 °C for 30 min. In the competitive binding experiments, cells were incubated with AgTx2-GFP (8 nM) and different concentrations (0.5–40 nM) of AgTx2 in complete medium at 37 °C for 30 min. In the experiments on the influence of channel state (open vs. closed) on ligand binding, cells were incubated with AgTx2-GFP (2–40 nM, 37 °C, 30 min) in a buffer (20 mM HEPES pH 7.4, 0.9 mM CaCl₂, 0.5 mM MgCl₂, and 0.1% BSA) containing either 150 mM KCl or 150 mM NaCl and 4 mM KCl.

Fluorescent images of cells were recorded with a laser scanning confocal microscope Leica-SP2 (Leica Microsystems GmbH, Wetzlar, Germany) equipped with a water immersion 63 \times /1.2 NA HCX PL APO objective (0.2 μ m lateral and 0.6 μ m axial resolutions). Fluorescence of AgTx2-GFP was excited at the 488 nm wavelength and recorded in the 495–535 nm range. Fluorescence of mKate2-K_v1.3 was excited at the 561 nm wavelength and recorded in the 650–700 nm range. Sequential scanning was used.

Fluorescent images were treated using ImageJ software (National Institutes of Health, Bethesda, MD, USA). Average fluorescence intensities of membrane-bound AgTx2-GFP and mKate2-K_v1.3 were determined for each examined cell and corrected for background signal, as described earlier [42], and their ratios R_i were calculated. The R_i values of 20–25 cells measured in the same conditions were averaged, producing the R_{av} values (\pm SD). The R_{av} values were plotted as a function of the concentration L of added AgTx2-GFP (Figure 5a) and fitted with the following equation:

$$R_{av} = R_m L / (K_d + L) \quad (5)$$

where R_m is R_{av} at the saturation of AgTx2-GFP binding.

The R_{av} values were plotted as a function of the concentration B of added AgTx2 at a fixed concentration L of AgTx2-GFP (Figure 5c) and fitted with the following equation:

$$R_{av} = R_{av0} / (1 + B / DC_{50}) \quad (6)$$

where DC_{50} is the concentration of AgTx2 displacing 50% of AgTx2-GFP from the complex with the K_v1.3 channel, and R_{av0} is R_{av} at $B = 0$.

The K_{ap} value of AgTx2 was calculated using the Cheng–Prusoff equation:

$$K_{ap} = DC_{50} / (1 + L / K_d) \quad (7)$$

All the measurements were repeated in two independent experiments, and data on the K_d and K_{av} were averaged and presented as means \pm SEM.

Supplementary Materials: The following supporting information can be downloaded at: <https://www.mdpi.com/article/10.3390/toxins15030229/s1>, Figure S1: Confocal imaging of AgTx2-GFP interactions with mKate2-tagged K_v1.3 channels transiently expressed in HEK293 cells. Figure S2: Confocal imaging of an interaction of AgTx2-GFP with Neuro 2A cells that did not express mKate2-K_v1.3. Figure S3: Time dependence of AgTx2-GFP binding to K_v1.3 channels on the membranes of Neuro 2A cells.

Author Contributions: Conceptualization, O.V.N. and A.V.F.; Methodology, N.A.O., S.P., J.T., A.A.I., O.V.N. and A.V.F.; Formal analysis, A.L.P., N.A.O., S.P., A.A.I., K.R.D., M.P.K. and O.V.N.; Investigation, A.L.P., N.A.O., S.P., A.A.I., K.R.D., S.A.Y. and O.V.N.; Writing—original draft, A.L.P., N.A.O., S.P., A.A.I., M.P.K., O.V.N. and A.V.F.; Writing—review & editing, J.T., M.P.K., O.V.N. and A.V.F.; Supervision, J.T., M.P.K., O.V.N. and A.V.F.; Project administration, M.P.K. and A.V.F.; Funding acquisition, N.A.O., S.P., J.T., A.A.I., K.R.D., O.V.N. and A.V.F. All authors have read and agreed to the published version of the manuscript.

Funding: This research was funded by the Russian Science Foundation (project 22-14-00406). The electrophysiological studies were supported by F.W.O. Vlaanderen grants GOA4919N, GOE7120N, and GOC2319N to J.T., as well as by F.W.O. Vlaanderen Grant 12W7822N to S.P.

Institutional Review Board Statement: The study was conducted in accordance with the Declaration of Helsinki. The use of the frogs was in accordance with license number LA1210239 of Toxicology and Pharmacology, KU Leuven, and was approved by the Ethical Committee for animal experiments of KU Leuven (P186/2019). Maximum efforts were made to minimize animal suffering and the number of animals used in the experiments.

Informed Consent Statement: Not applicable.

Data Availability Statement: The data presented in this study are available on request from the corresponding author. The data are not publicly available due to local regulations.

Acknowledgments: The research was performed using the facilities of the Interdisciplinary Scientific and Educational School of Moscow University “Molecular Technologies of the Living Systems and Synthetic Biology”. The authors would like to thank Alexander Vassilevski for the gift of scorpion venoms and helpful assistance.

Conflicts of Interest: The authors declare no conflict of interest. The funders had no role in the design of the study; in the collection, analyses, or interpretation of data; in the writing of the manuscript; or in the decision to publish the results.

References

1. Kuzmenkov, A.I.; Grishin, E.V.; Vassilevski, A.A. Diversity of Potassium Channel Ligands: Focus on Scorpion Toxins. *Biochemistry* **2015**, *80*, 1764–1799. [[CrossRef](#)] [[PubMed](#)]
2. Rodríguez de la Vega, R.C.; Possani, L.D. Current Views on Scorpion Toxins Specific for K⁺-Channels. *Toxicon* **2004**, *43*, 865–875. [[CrossRef](#)] [[PubMed](#)]
3. Kuang, Q.; Purhonen, P.; Hebert, H. Structure of Potassium Channels. *Cell. Mol. Life Sci.* **2015**, *72*, 3677–3693. [[CrossRef](#)] [[PubMed](#)]
4. Fan, Y.; Zong-Yun, C.; Ying-Liang, W. Unique Interactions between Scorpion Toxins and Small Conductance Ca²⁺-Activated Potassium Channels. *Acta Physiol. Sin.* **2015**, *67*, 255–260. [[CrossRef](#)]
5. Gutman, G.A.; Chandy, K.G.; Grissmer, S.; Lazdunski, M.; McKinnon, D.; Pardo, L.A.; Robertson, G.A.; Rudy, B.; Sanguinetti, M.C.; Stühmer, W.; et al. International Union of Pharmacology. LIII. Nomenclature and Molecular Relationships of Voltage-Gated Potassium Channels. *Pharmacol. Rev.* **2005**, *57*, 473–508. [[CrossRef](#)] [[PubMed](#)]
6. Mouhat, S.; Visan, V.; Ananthakrishnan, S.; Wulff, H.; Andreotti, N.; Grissmer, S.; Darbon, H.; De Waard, M.; Sabatier, J.-M. K⁺ Channel Types Targeted by Synthetic OSK1, a Toxin from Orthochirus Scrobiculosus Scorpion Venom. *Biochem. J.* **2005**, *385*, 95–104. [[CrossRef](#)]
7. Kuzmenkov, A.I.; Nekrasova, O.V.; Kudryashova, K.S.; Peigneur, S.; Tytgat, J.; Stepanov, A.V.; Kirpichnikov, M.P.; Grishin, E.V.; Feofanov, A.V.; Vassilevski, A.A. Fluorescent Protein-Scorpion Toxin Chimera Is a Convenient Molecular Tool for Studies of Potassium Channels. *Sci. Rep.* **2016**, *6*, 33314. [[CrossRef](#)]
8. Mouhat, S.; Teodorescu, G.; Homerick, D.; Visan, V.; Wulff, H.; Wu, Y.; Grissmer, S.; Darbon, H.; De Waard, M.; Sabatier, J.-M. Pharmacological Profiling of Orthochirus Scrobiculosus Toxin 1 Analogs with a Trimmed N-Terminal Domain. *Mol. Pharmacol.* **2006**, *69*, 354–362. [[CrossRef](#)]
9. Restano-Cassulini, R.; Korolkova, Y.V.; Diochot, S.; Gurrola, G.; Guasti, L.; Possani, L.D.; Lazdunski, M.; Grishin, E.V.; Arcangeli, A.; Wanke, E. Species Diversity and Peptide Toxins Blocking Selectivity of Ether-a-Go-Go-Related Gene Subfamily K⁺ Channels in the Central Nervous System. *Mol. Pharmacol.* **2006**, *69*, 1673–1683. [[CrossRef](#)]

10. Garcia, M.L.; Garcia-Calvo, M.; Hidalgo, P.; Lee, A.; MacKinnon, R. Purification and Characterization of Three Inhibitors of Voltage-Dependent K⁺ Channels from *Leiurus Quinquestriatus* Var. *Hebraeus* Venom. *Biochemistry* **1994**, *33*, 6834–6839. [[CrossRef](#)]
11. Varga, Z.; Gurrola-Briones, G.; Papp, F.; Rodriguez De La Vega, R.C.; Pedraza-Alva, G.; Tajhya, R.B.; Gaspar, R.; Cardenas, L.; Rosenstein, Y.; Beeton, C.; et al. Vm24, a Natural Immunosuppressive Peptide, Potently and Selectively Blocks Kv1.3 Potassium Channels of Human T Cells. *Mol. Pharmacol.* **2012**, *82*, 372–382. [[CrossRef](#)] [[PubMed](#)]
12. Kuzmenkov, A.I.; Nekrasova, O.V.; Peigneur, S.; Tabakmakher, V.M.; Gigolaev, A.M.; Fradkov, A.F.; Kudryashova, K.S.; Chugunov, A.O.; Efremov, R.G.; Tytgat, J.; et al. Kv1.2 Channel-Specific Blocker from *Mesobuthus Eupeus* Scorpion Venom: Structural Basis of Selectivity. *Neuropharmacology* **2018**, *143*, 228–238. [[CrossRef](#)]
13. Zhao, Y.; Chen, Z.; Cao, Z.; Li, W.; Wu, Y. Diverse Structural Features of Potassium Channels Characterized by Scorpion Toxins as Molecular Probes. *Molecules* **2019**, *24*, 2045. [[CrossRef](#)] [[PubMed](#)]
14. Ortiz, E.; Possani, L.D. Scorpion Toxins to Unravel the Conundrum of Ion Channel Structure and Functioning. *Toxicon* **2018**, *150*, 17–27. [[CrossRef](#)]
15. Zundler, S.; Caioni, M.; Müller, M.; Strauch, U.; Kunst, C.; Woelfel, G. K⁺ Channel Inhibition Differentially Regulates Migration of Intestinal Epithelial Cells in Inflamed vs. Non-Inflamed Conditions in a PI3K/Akt-Mediated Manner. *PLoS ONE* **2016**, *11*, e0147736. [[CrossRef](#)]
16. Gossen, D.; Gesquière, J.C.; Tastenoy, M.; De Neef, P.; Waelbroeck, M.; Christophe, J. Characterization and Regulation of the Expression of Scyllatoxin (Leiurotoxin I) Receptors in the Human Neuroblastoma Cell Line NB-OK 1. *FEBS Lett.* **1991**, *285*, 271–274. [[CrossRef](#)]
17. Veytia-Bucheli, J.I.; Jiménez-Vargas, J.M.; Melchy-Pérez, E.I.; Sandoval-Hernández, M.A.; Possani, L.D.; Rosenstein, Y. Kv1.3 Channel Blockade with the Vm24 Scorpion Toxin Attenuates the CD4⁺ Effector Memory T Cell Response to TCR Stimulation. *Cell Commun. Signal.* **2018**, *16*, 45. [[CrossRef](#)] [[PubMed](#)]
18. Nicolazzo, J.A.; Pan, Y.; Di Stefano, I.; Choy, K.H.C.; Reddiar, S.B.; Low, Y.L.; Wai, D.C.C.; Norton, R.S.; Jin, L. Blockade of Microglial Kv1.3 Potassium Channels by the Peptide HsTX1[R14A] Attenuates Lipopolysaccharide-Mediated Neuroinflammation. *J. Pharm. Sci.* **2022**, *111*, 638–647. [[CrossRef](#)]
19. Banerjee, A.; Lee, A.; Campbell, E.; MacKinnon, R. Structure of a Pore-Blocking Toxin in Complex with a Eukaryotic Voltage-Dependent K⁺ Channel. *Elife* **2013**, *2*, e00594. [[CrossRef](#)]
20. Qiu, S.; Yi, H.; Liu, H.; Cao, Z.; Wu, Y.; Li, W. Molecular Information of Charybdotoxin Blockade in the Large Conductance Calcium-Activated Potassium Channel. *J. Chem. Inf. Model.* **2009**, *49*, 1831–1838. [[CrossRef](#)]
21. Koeberle, P.D.; Schlichter, L.C. Targeting KV Channels Rescues Retinal Ganglion Cells in Vivo Directly and by Reducing Inflammation. *Channels* **2010**, *4*, 337. [[CrossRef](#)] [[PubMed](#)]
22. Menteyne, A.; Levavasseur, F.; Audinat, E.; Avignone, E. Predominant Functional Expression of Kv1.3 by Activated Microglia of the Hippocampus after Status Epilepticus. *PLoS ONE* **2009**, *4*, e6770. [[CrossRef](#)] [[PubMed](#)]
23. Cañas, C.A.; Castaño-Valencia, S.; Castro-Herrera, F. Pharmacological Blockade of KV1.3 Channel as a Promising Treatment in Autoimmune Diseases. *J. Transl. Autoimmun.* **2022**, *5*, 100146. [[CrossRef](#)] [[PubMed](#)]
24. Comes, N.; Bielanska, J.; Vallejo-Gracia, A.; Serrano-Albarrás, A.; Marruecos, L.; Gómez, D.; Soler, C.; Condom, E.; Ramón y Cajal, S.; Hernández-Losa, J.; et al. The Voltage-Dependent K(+) Channels Kv1.3 and Kv1.5 in Human Cancer. *Front. Physiol.* **2013**, *4*, 283. [[CrossRef](#)]
25. Feske, S.; Wulff, H.; Skolnik, E.Y. Ion Channels in Innate and Adaptive Immunity. *Annu. Rev. Immunol.* **2015**, *33*, 291–353. [[CrossRef](#)]
26. Kazama, I. Targeting Lymphocyte Kv1.3-Channels to Suppress Cytokine Storm in Severe COVID-19: Can It Be a Novel Therapeutic Strategy? *Drug Discov. Ther.* **2020**, *14*, 143–144. [[CrossRef](#)]
27. Jen, J.C.; Wan, J. Episodic Ataxias. *Handb. Clin. Neurol.* **2018**, *155*, 205–215. [[CrossRef](#)]
28. D’adamo, M.C.; Liantonio, A.; Rolland, J.F.; Pessia, M.; Imbrici, P. Kv1.1 Channelopathies: Pathophysiological Mechanisms and Therapeutic Approaches. *Int. J. Mol. Sci.* **2020**, *21*, 2935. [[CrossRef](#)]
29. Serrano-Albarrás, A.; Cirera-Rocosa, S.; Sastre, D.; Estadella, I.; Felipe, A. Fighting Rheumatoid Arthritis: Kv1.3 as a Therapeutic Target. *Biochem. Pharmacol.* **2019**, *165*, 214–220. [[CrossRef](#)]
30. Peter Muiruri, K.; Zhong, J.; Yao, B.; Lai, R.; Luo, L. Bioactive Peptides from Scorpion Venoms: Therapeutic Scaffolds and Pharmacological Tools. *Chin. J. Nat. Med.* **2023**, *21*, 19–35. [[CrossRef](#)]
31. Bartok, A.; Fehér, K.; Bodor, A.; Rákosi, K.; Tóth, G.K.; Kövér, K.E.; Panyi, G.; Varga, Z. An Engineered Scorpion Toxin Analogue with Improved Kv1.3 Selectivity Displays Reduced Conformational Flexibility. *Sci. Rep.* **2015**, *5*, 18397. [[CrossRef](#)] [[PubMed](#)]
32. Rashid, M.H.; Heinzemann, G.; Huq, R.; Tajhya, R.B.; Chang, S.C.; Chhabra, S.; Pennington, M.W.; Beeton, C.; Norton, R.S.; Kuyucak, S. A Potent and Selective Peptide Blocker of the Kv1.3 Channel: Prediction from Free-Energy Simulations and Experimental Confirmation. *PLoS ONE* **2013**, *8*, e78712. [[CrossRef](#)] [[PubMed](#)]
33. Varga, Z.; Tajti, G.; Panyi, G. The Kv1.3 K⁺ Channel in the Immune System and Its “Precision Pharmacology” Using Peptide Toxins. *Biol. Futur.* **2021**, *72*, 75–83. [[CrossRef](#)] [[PubMed](#)]
34. Takacs, Z.; Touts, M.; Kollwe, A.; Johnson, E.; Cuello, L.G.; Driessens, G.; Biancalana, M.; Koide, A.; Ponte, C.G.; Perozo, E.; et al. A Designer Ligand Specific for Kv1.3 Channels from a Scorpion Neurotoxin-Based Library. *Proc. Natl. Acad. Sci. USA* **2009**, *106*, 22211–22216. [[CrossRef](#)] [[PubMed](#)]

35. Kuzmenkov, A.I.; Vassilevski, A.A. Labelled Animal Toxins as Selective Molecular Markers of Ion Channels: Applications in Neurobiology and Beyond. *Neurosci. Lett.* **2018**, *679*, 15–23. [[CrossRef](#)] [[PubMed](#)]
36. Koschak, A.; Koch, R.O.; Liu, J.; Kaczorowski, G.J.; Reinhart, P.H.; Garcia, M.L.; Knaus, H.G. [125I]Iberitoxin-D19Y/Y36F, the First Selective, High Specific Activity Radioligand for High-Conductance Calcium-Activated Potassium Channels. *Biochemistry* **1997**, *36*, 1943–1952. [[CrossRef](#)]
37. Koschak, A.; Bugianesi, R.M.; Mitterdorfer, J.; Kaczorowski, G.J.; Garcia, M.L.; Knaus, H.G. Subunit Composition of Brain Voltage-Gated Potassium Channels Determined by Hongotoxin-1, a Novel Peptide Derived from Centruroides Limbatus Venom. *J. Biol. Chem.* **1998**, *273*, 2639–2644. [[CrossRef](#)]
38. Knaus, H.G.; Schwarzer, C.; Koch, R.O.A.; Eberhart, A.; Kaczorowski, G.J.; Glossmann, H.; Wunder, F.; Pongs, O.; Garcia, M.L.; Sperk, G. Distribution of High-Conductance Ca(2+)-Activated K⁺ Channels in Rat Brain: Targeting to Axons and Nerve Terminals. *J. Neurosci.* **1996**, *16*, 955–963. [[CrossRef](#)]
39. Freudenthaler, G.; Axmann, M.; Schindler, H.; Pragl, B.; Knaus, H.G.; Schütz, G.J. Ultrasensitive Pharmacological Characterisation of the Voltage-Gated Potassium Channel K(V)1.3 Studied by Single-Molecule Fluorescence Microscopy. *Histochem. Cell Biol.* **2002**, *117*, 197–202. [[CrossRef](#)]
40. Coyote-Maestas, W.; Nedrud, D.; Suma, A.; He, Y.; Matreyek, K.A.; Fowler, D.M.; Carnevale, V.; Myers, C.L.; Schmidt, D. Probing Ion Channel Functional Architecture and Domain Recombination Compatibility by Massively Parallel Domain Insertion Profiling. *Nat. Commun.* **2021**, *12*, 7114. [[CrossRef](#)]
41. Wai, D.C.C.; Naseem, M.U.; Mocsár, G.; Babu Reddiar, S.; Pan, Y.; Csoti, A.; Hajdu, P.; Nowell, C.; Nicolazzo, J.A.; Panyi, G.; et al. A Fluorescent Peptide Toxin for Selective Visualization of the Voltage-Gated Potassium Channel Kv1.3. *Bioconjug. Chem.* **2022**, *33*, 2197–2212. [[CrossRef](#)]
42. Orlov, N.A.; Ignatova, A.A.; Kryukova, E.V.; Yakimov, S.A.; Kirpichnikov, M.P.; Nekrasova, O.V.; Feofanov, A.V. Combining MKate2-Kv1.3 Channel and Atto488-Hongotoxin for the Studies of Peptide Pore Blockers on Living Eukaryotic Cells. *Toxins* **2022**, *14*, 858. [[CrossRef](#)]
43. Denisova, K.R.; Orlov, N.A.; Yakimov, S.A.; Kirpichnikov, M.P.; Feofanov, A.V.; Nekrasova, O.V. Atto488-Agitoxin 2-A Fluorescent Ligand with Increased Selectivity for Kv1.3 Channel Binding Site. *Bioengineering* **2022**, *9*, 295. [[CrossRef](#)] [[PubMed](#)]
44. Kudryashova, K.S.; Nekrasova, O.V.; Kuzmenkov, A.I.; Vassilevski, A.A.; Ignatova, A.A.; Korolkova, Y.V.; Grishin, E.V.; Kirpichnikov, M.P.; Feofanov, A.V. Fluorescent System Based on Bacterial Expression of Hybrid KcsA Channels Designed for Kv1.3 Ligand Screening and Study. *Anal. Bioanal. Chem.* **2013**, *405*, 2379–2389. [[CrossRef](#)] [[PubMed](#)]
45. Denisova, K.R.; Orlov, N.A.; Yakimov, S.A.; Kryukova, E.A.; Dolgikh, D.A.; Kirpichnikov, M.P.; Feofanov, A.V.; Nekrasova, O.V. GFP-Margatoxin, a Genetically Encoded Fluorescent Ligand to Probe Affinity of Kv1.3 Channel Blockers. *Int. J. Mol. Sci.* **2022**, *23*, 1724. [[CrossRef](#)] [[PubMed](#)]
46. Nekrasova, O.V.; Primak, A.L.; Ignatova, A.A.; Novoseletsky, V.N.; Geras'kina, O.V.; Kudryashova, K.S.; Yakimov, S.A.; Kirpichnikov, M.P.; Arseniev, A.S.; Feofanov, A.V. N-Terminal Tagging with GFP Enhances Selectivity of Agitoxin 2 to Kv1.3-Channel Binding Site. *Toxins* **2020**, *12*, 802. [[CrossRef](#)]
47. Primak, A.L.; Skutel, M.A.; Nekrasova, O.V.; Arseniev, A.S.; Kirpichnikov, M.P.; Feofanov, A.V. Kv1 Potassium Channel Ligands Based on Hongotoxin 1 and Red Fluorescent Protein. *Russ. J. Bioorg. Chem.* **2020**, *46*, 1011–1017. [[CrossRef](#)]
48. Merzlyak, E.M.; Goedhart, J.; Shcherbo, D.; Bulina, M.E.; Shcheglov, A.S.; Fradkov, A.F.; Gaintzeva, A.; Lukyanov, K.A.; Lukyanov, S.; Gadella, T.W.J.; et al. Bright Monomeric Red Fluorescent Protein with an Extended Fluorescence Lifetime. *Nat. Methods* **2007**, *4*, 555–557. [[CrossRef](#)]
49. Zhang, G.; Gurtu, V.; Kain, S.R. An Enhanced Green Fluorescent Protein Allows Sensitive Detection of Gene Transfer in Mammalian Cells. *Biochem. Biophys. Res. Commun.* **1996**, *227*, 707–711. [[CrossRef](#)]
50. Nekrasova, O.V.; Volynitseva, A.D.; Kudryashova, K.S.; Novoseletsky, V.N.; Lyapina, E.A.; Illarionova, A.V.; Yakimov, S.A.; Korolkova, Y.V.; Shaitan, K.V.; Kirpichnikov, M.P.; et al. Complexes of Peptide Blockers with Kv1.6 Pore Domain: Molecular Modeling and Studies with KcsA-Kv1.6 Channel. *J. Neuroimmune Pharmacol.* **2017**, *12*, 260–276. [[CrossRef](#)]
51. Kuzmenkov, A.I.; Vassilevski, A.A.; Kudryashova, K.S.; Nekrasova, O.V.; Peigneur, S.; Tytgat, J.; Feofanov, A.V.; Kirpichnikov, M.P.; Grishin, E.V. Variability of Potassium Channel Blockers in Mesobuthus Eupeus Scorpion Venom with Focus on Kv1.1: An Integrated Transcriptomic and Proteomic Study. *J. Biol. Chem.* **2015**, *290*, 12195–12209. [[CrossRef](#)]
52. Kudryashova, K.S.; Nekrasova, O.V.; Kirpichnikov, M.P.; Feofanov, A.V. Chimeras of KcsA and Kv1 as a Bioengineering Tool to Study Voltage-Gated Potassium Channels and Their Ligands. *Biochem. Pharmacol.* **2021**, *190*, 114646. [[CrossRef](#)] [[PubMed](#)]
53. Anangi, R.; Koshy, S.; Huq, R.; Beeton, C.; Chuang, W.J.; King, G.F. Recombinant Expression of Margatoxin and Agitoxin-2 in Pichia Pastoris: An Efficient Method for Production of KV1.3 Channel Blockers. *PLoS ONE* **2012**, *7*, e52965. [[CrossRef](#)]
54. Hao, J.; Padilla, F.; Dandonneau, M.; Lavebratt, C.; Lesage, F.; Noël, J.; Delmas, P. Kv1.1 Channels Act as Mechanical Brake in the Senses of Touch and Pain. *Neuron* **2013**, *77*, 899–914. [[CrossRef](#)]
55. Pimentel, C.; M'Barek, S.; Visan, V.; Grissmer, S.; Sampieri, F.; Sabatier, J.-M.; Darbon, H.; Fajloun, Z. Chemical Synthesis and 1H-NMR 3D Structure Determination of AgTx2-MTX Chimera, a New Potential Blocker for Kv1.2 Channel, Derived from MTX and AgTx2 Scorpion Toxins. *Protein Sci.* **2007**, *17*, 107–118. [[CrossRef](#)] [[PubMed](#)]
56. Attali, B.; Romey, G.; Honore, E.; Schmid-Alliana, A.; Mattei, M.G.; Lesage, F.; Ricard, P.; Barhanin, J.; Lazdunski, M. Cloning, Functional Expression, and Regulation of Two K⁺ Channels in Human T Lymphocytes. *J. Biol. Chem.* **1992**, *267*, 8650–8657. [[CrossRef](#)]

57. Hu, L.; Pennington, M.; Jiang, Q.; Whartenby, K.A.; Calabresi, P.A. Characterization of the Functional Properties of the Voltage-Gated Potassium Channel Kv1.3 in Human CD4+ T Lymphocytes. *J. Immunol.* **2007**, *179*, 4563–4570. [[CrossRef](#)]
58. Fomina, A.F.; Nguyen, H.M.; Wulff, H. Kv1.3 Inhibition Attenuates Neuroinflammation through Disruption of Microglial Calcium Signaling. *Channels* **2021**, *15*, 67–78. [[CrossRef](#)] [[PubMed](#)]
59. Teisseyre, A.; Palko-Labuz, A.; Sroda-Pomianek, K.; Michalak, K. Voltage-Gated Potassium Channel Kv1.3 as a Target in Therapy of Cancer. *Front. Oncol.* **2019**, *9*, 933. [[CrossRef](#)] [[PubMed](#)]
60. Pérez-Verdaguer, M.; Capera, J.; Serrano-Novillo, C.; Estadella, I.; Sastre, D.; Felipe, A. The Voltage-Gated Potassium Channel Kv1.3 Is a Promising Multitherapeutic Target against Human Pathologies. *Expert. Opin. Ther. Targets* **2016**, *20*, 577–591. [[CrossRef](#)]
61. Paulhus, K.; Ammerman, L.; Glasscock, E. Clinical Spectrum of KCNA1 Mutations: New Insights into Episodic Ataxia and Epilepsy Comorbidity. *Int. J. Mol. Sci.* **2020**, *21*, 2802. [[CrossRef](#)] [[PubMed](#)]
62. Robbins, C.A.; Tempel, B.L. Kv1.1 and Kv1.2: Similar Channels, Different Seizure Models. *Epilepsia* **2012**, *53* (Suppl. S1), 134–141. [[CrossRef](#)] [[PubMed](#)]
63. Al-Sabi, A.; Daly, D.; Hoefer, P.; Kinsella, G.K.; Metais, C.; Pickering, M.; Herron, C.; Kaza, S.K.; Nolan, K.; Dolly, J.O. A Rational Design of a Selective Inhibitor for Kv1.1 Channels Prevalent in Demyelinated Nerves That Improves Their Impaired Axonal Conduction. *J. Med. Chem.* **2017**, *60*, 2245–2256. [[CrossRef](#)] [[PubMed](#)]
64. Otuyemi, B.; Jackson, T.; Ma, R.; Monteiro, A.R.; Seifi, M.; Swinny, J.D. Domain and Cell Type-Specific Immunolocalisation of Voltage-Gated Potassium Channels in the Mouse Striatum. *J. Chem. Neuroanat.* **2023**, *128*, 102233. [[CrossRef](#)]
65. Bindels, D.S.; Haarbosch, L.; van Weeren, L.; Postma, M.; Wiese, K.E.; Mastop, M.; Aumonier, S.; Gotthard, G.; Royant, A.; Hink, M.A.; et al. MScarlet: A Bright Monomeric Red Fluorescent Protein for Cellular Imaging. *Nat. Methods* **2017**, *14*, 53–56. [[CrossRef](#)] [[PubMed](#)]
66. Zarowny, L.; Clavel, D.; Johansson, R.; Duarte, K.; Depernet, H.; Dupuy, J.; Baker, H.; Brown, A.; Royant, A.; Campbell, R.E. Cyan Fluorescent Proteins Derived from mNeonGreen. *Protein Eng. Des. Sel.* **2022**, *35*, gzac004. [[CrossRef](#)]
67. Hirano, M.; Ando, R.; Shimozone, S.; Sugiyama, M.; Takeda, N.; Kurokawa, H.; Deguchi, R.; Endo, K.; Haga, K.; Takai-Todaka, R.; et al. A Highly Photostable and Bright Green Fluorescent Protein. *Nat. Biotechnol.* **2022**, *40*, 1132–1142. [[CrossRef](#)]
68. Nekrasova, O.; Kudryashova, K.; Fradkov, A.; Yakimov, S.; Savelieva, M.; Kirpichnikov, M.; Feofanov, A. Straightforward Approach to Produce Recombinant Scorpion Toxins—Pore Blockers of Potassium Channels. *J. Biotechnol.* **2017**, *241*, 127–135. [[CrossRef](#)]
69. Koren, G.; Liman, E.R.; Logothetis, D.E.; Nadal-Ginard, B.; Hess, P. Gating Mechanism of a Cloned Potassium Channel Expressed in Frog Oocytes and Mammalian Cells. *Neuron* **1990**, *4*, 39–51. [[CrossRef](#)]
70. Peigneur, S.; Cheneval, O.; Maiti, M.; Leipold, E.; Heinemann, S.H.; Lescrinier, E.; Herdewijn, P.; de Lima, M.E.; Craik, D.J.; Schroeder, C.I.; et al. Where Cone Snails and Spiders Meet: Design of Small Cyclic Sodium-Channel Inhibitors. *FASEB J.* **2019**, *33*, 3693–3703. [[CrossRef](#)]
71. Vriens, K.; Peigneur, S.; de Coninck, B.; Tytgat, J.; Cammue, B.P.A.; Thevissen, K. The Antifungal Plant Defensin AtPDF2.3 from *Arabidopsis thaliana* Blocks Potassium Channels. *Sci. Rep.* **2016**, *6*, 32121. [[CrossRef](#)] [[PubMed](#)]
72. Peigneur, S.; Billen, B.; Derua, R.; Waelkens, E.; Debaveye, S.; Béress, L.; Tytgat, J. A Bifunctional Sea Anemone Peptide with Kunitz Type Protease and Potassium Channel Inhibiting Properties. *Biochem. Pharmacol.* **2011**, *82*, 81–90. [[CrossRef](#)] [[PubMed](#)]

Disclaimer/Publisher’s Note: The statements, opinions and data contained in all publications are solely those of the individual author(s) and contributor(s) and not of MDPI and/or the editor(s). MDPI and/or the editor(s) disclaim responsibility for any injury to people or property resulting from any ideas, methods, instructions or products referred to in the content.